

# The complex velocity distribution of galaxies in Abell 1689: implications for mass modelling

E. L. Łokas<sup>1</sup>, F. Prada<sup>2</sup>, R. Wojtak<sup>3</sup>, M. Moles<sup>2</sup> and S. Gottlöber<sup>4</sup>

<sup>1</sup>*Nicolaus Copernicus Astronomical Center, Bartycka 18, 00-716 Warsaw, Poland; lokas@camk.edu.pl,*

<sup>2</sup>*Instituto de Astrofísica de Andalucía (CSIC), Apartado Correos 3005, E-18080 Granada, Spain*

<sup>3</sup>*Astronomical Observatory, Jagiellonian University, Orła 171, 30-244 Cracow, Poland*

<sup>4</sup>*Astrophysikalisches Institut Potsdam, An der Sternwarte 16, 14482 Potsdam, Germany*

2 September 2018

## ABSTRACT

The Abell 1689 galaxy cluster has recently become a subject of intensive study. Thanks to its intermediate redshift ( $z = 0.183$ ) its mass distribution can be reconstructed using numerous methods including gravitational lensing, galaxy kinematics and X-ray imaging. The methods used to yield conflicting mass estimates in the past and recently the cluster mass distribution has been claimed to be in conflict with standard CDM scenarios due to rather large concentration and steep mass profile obtained from detailed studies of Broadhurst et al. using lensing. By studying in detail the kinematics of about 200 galaxies with measured redshifts in the vicinity of the cluster we show that the cluster is probably surrounded by a few structures, quite distant from each other, but aligned along the line of sight. We support our arguments by referring to cosmological  $N$ -body simulations and showing explicitly that distant, non-interacting haloes can produce entangled multi-peak line-of-sight velocity distributions similar to that in A1689. We conclude that it is difficult to estimate the cluster mass reliably from galaxy kinematics, but the value we obtain after applying a simple cut-off in velocity agrees roughly with the mass estimated from lensing. The complicated mass distribution around the cluster may however increase the uncertainty in the determination of the density profile shape obtained with weak lensing.

**Key words:** methods:  $N$ -body simulations – methods: analytical – galaxies: clusters: general – galaxies: clusters: individual: A1689 – cosmology: dark matter

## 1 INTRODUCTION

The increasing amount of data on Abell 1689, a cluster of galaxies at  $z=0.183$ , has recently motivated several detailed analyses of its dynamical status and mass distribution. As the largest known gravitational lensing object it has been studied in detail by Broadhurst et al. (2005a, 2005b) who found that the inferred mass distribution is much steeper compared to what is expected for dark matter haloes forming in currently available cosmological  $N$ -body simulations. In particular they find the concentration parameter of the best-fitting NFW (Navarro, Frenk & White 1997) profile of the cluster to be between  $c = 8$  and  $c = 14$  depending on projected radius to which the mass distribution was studied. The smaller value was obtained from the strong lensing results in the inner part of the cluster, while the larger value was found when the study was extended to a scale of 2 Mpc using the results from weak lensing. The larger value seems rather high for the estimated mass of  $2 \times 10^{15} M_{\odot}$  compared to the expected value of  $c = 5$  for haloes of this mass as found in cosmological  $N$ -body simulations (e.g. Bullock et

al. 2001). The discrepancy has led Oguri et al. (2005) to claim that the mass distribution in A1689 may be in conflict with the standard cold dark matter (CDM) scenarios for structure formation. They have shown that the disagreement can be partially reduced if the uncertainties in the parameter estimation due to the possible triaxiality of the halo are properly taken into account.

The X-ray data for Abell 1689 obtained with the XMM-Newton telescope have been analyzed by Andersson & Madejski (2004). The X-ray gas surface brightness distribution appears rather regular and smooth. However, a closer inspection reveals that the gas temperature profile is highly asymmetric and the gas mass fraction is lower than usual, which may point towards a perturbed structure. Moreover, the total mass inferred from the X-ray analysis gives a value twice as small as that found from gravitational lensing.

Kinematical analysis of the cluster galaxies shows even larger discrepancies. The redshift survey performed by Teague, Carter & Gray (1990) led to the identification of a few structures along the line of sight and an estimate of

2355 km s<sup>-1</sup> for the velocity dispersion of the cluster members. Struble & Rood (1999) estimate the cluster dispersion to be 1989 km s<sup>-1</sup> using the same data. Girardi et al. (1997) applied the wavelet analysis to the same data and detected even more substructure. Although their estimate for the main cluster velocity dispersion was 1429 km s<sup>-1</sup>, they calculated the mass by adding the masses of two main substructures with low velocity dispersions of the order of 300-400 km s<sup>-1</sup> which led to the value of about  $2 \times 10^{14} M_{\odot}$ , an order of magnitude lower than the mass obtained from the lensing studies.

In this Letter we reanalyze the velocity distribution of galaxies in the field of A1689 using the larger sample now available. We confirm that the cluster indeed has a complex structure in velocity space, strongly indicating the presence of dynamically independent structures along the line of sight. By imposing different cut-offs in velocity we show how the cluster mass estimate can change by a large factor, which illustrates the difficulty in inferring it from the kinematical data. The complicated mass distribution around the cluster may also affect mass estimates done with other methods. We refer to cosmological  $N$ -body simulations in order to demonstrate that distant haloes positioned along the line of observations can indeed produce line-of-sight velocity distributions similar to the one in A1689. Therefore any estimate of concentration for an object in such environment may be biased by an error not associated with the method of mass determination but due to the presence of foreground and background structures.

## 2 VELOCITY DISTRIBUTION OF GALAXIES IN A1689

We have searched the NED database for galaxies with redshifts  $z = 0.1832 \pm 0.05$  and located at distances smaller than 2 Mpc from the cluster centre assumed to be at RA=13<sup>h</sup>11<sup>m</sup>30.3<sup>s</sup>, Dec=-01°20′53″ (J2000). It corresponds to the position of the elliptical galaxy closest to the centre of the main structure detected by Girardi et al. (1997). It is also within 100 kpc from the centre of X-ray gas surface brightness distribution. The redshift data for galaxies thus chosen come mainly from surveys by Teague et al. (1990), Balogh et al. (2002) and Duc et al. (2002).

The line-of-sight velocities of 192 galaxies in the reference frame of the cluster as a function of distance from the cluster centre are shown in the upper left panel of Fig. 1. The colours code the probable membership of the galaxies in different groups separated in velocity space. The division has been made by a simple cut-off in constant  $v$ . Separating first galaxies with  $|v| > 6000$  km s<sup>-1</sup> we get a group of 15 galaxies marked by red dots. The other two groups with  $3000$  km s<sup>-1</sup>  $< |v| < 6000$  km s<sup>-1</sup> are marked with green and blue respectively for the positive (35 galaxies) and negative velocities (12 galaxies). The remaining 130 galaxies with  $|v| < 3000$  km s<sup>-1</sup> are marked with black dots and correspond most probably to the main body of the cluster. The same colour coding applies to the velocity distribution histogram (number of galaxies per velocity bin of size 1000 km s<sup>-1</sup>) shown in the upper right panel of the Figure. The lower left panel of the Figure shows the position of the galaxies belonging to each group on the plane of the sky; the positions overlap indicating that the groups lie along the line of sight.

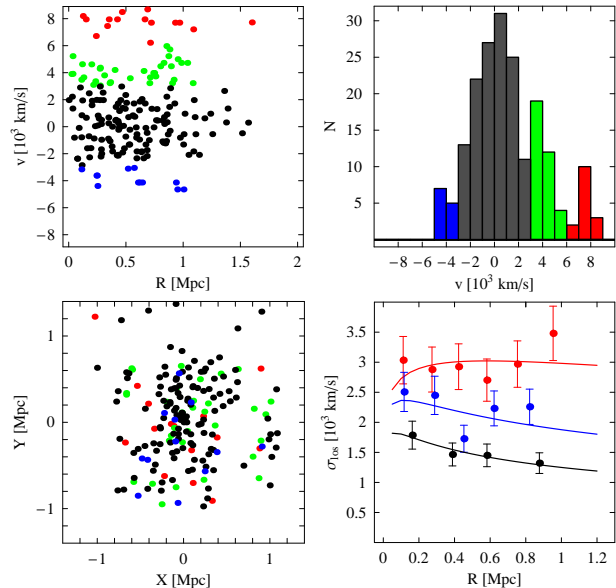


**Figure 1.** Projected distributions of galaxies in the vicinity of A1689. Upper left panel: line-of-sight velocities of galaxies as a function of projected distance from cluster centre divided into different velocity bins  $|v| > 6000$  km s<sup>-1</sup> (red),  $3000$  km s<sup>-1</sup>  $< |v| < 6000$  km s<sup>-1</sup> (green and blue respectively for the positive and negative velocities),  $|v| < 3000$  km s<sup>-1</sup> (black). Lower left panel: positions of the groups of galaxies on the surface of the sky. Upper right panel: the histogram of the line-of-sight velocity distribution plotting the number of galaxies per velocity bin of size 1000 km s<sup>-1</sup> with colour coding as in previous plots. Lower right panel: line-of-sight velocity dispersion profiles obtained for all galaxies (red), galaxies with  $|v| < 6000$  km s<sup>-1</sup> (blue) and galaxies with  $|v| < 3000$  km s<sup>-1</sup> (black). Solid lines show the best-fitting solutions of the Jeans equation.

The histogram shown in the upper right panel of Fig. 1 is similar to that in Fig. 1 of Girardi et al. (1997), but the identification of structure is somewhat different. In particular, the green, red and blue peaks in our histogram are the same as those at  $cz = 60, 64$  and  $52 \times 10^3$  km s<sup>-1</sup> respectively in their Figure, but we do not see the structures with velocities close to the cluster mean, which they identified as S2 and S3, as separate. Although some fluctuations in the number of galaxies can be seen in this region when we plot the histogram with better resolution, we do not think they are significant. The two upper panels of Fig. 1 show qualitatively that the cluster has a complicated structure in velocity space, at variance with what is expected for relaxed, isolated objects.

The lower right panel of Fig. 1 plots the velocity dispersion profiles calculated using different galaxy samples. The red profile was obtained from the total sample of 192 galaxies, for the blue one the galaxies with  $|v| > 6000$  km s<sup>-1</sup> with respect to the cluster mean were removed, and the black one is for galaxies with  $|v| < 3000$  km s<sup>-1</sup>. The data points were calculated with 30 galaxies per bin and assigned standard sampling errors (see Lokas & Mamon 2003). The profiles can be used as a quantitative measure of the mass of the structure. Assuming that the galaxies trace the overall NFW mass distribution in the cluster and have isotropic orbits we can estimate the parameters of the NFW profile, the virial mass  $M_v$  and concentration  $c$  by fitting the velocity dispersion data to the solutions of the Jeans equation

**Table 1.** Best-fitting virial masses and concentrations of A1689 estimated from velocity dispersion profiles for different galaxy samples.

sample	$M_v [10^{15} M_\odot]$	$r_v$ [Mpc]	$c$
all galaxies	33	8.3	7.3
$ v  < 6000 \text{ km s}^{-1}$	7.1	5.0	22
$ v  < 3000 \text{ km s}^{-1}$	2.6	3.5	28

$$\sigma_{\text{los}}^2(R) = \frac{2}{I(R)} \int_R^\infty \frac{\nu \sigma_r^2(r) r}{\sqrt{r^2 - R^2}} dr, \quad (1)$$

where  $\nu(r)$  and  $I(R)$  are the 3D and the surface distribution of the tracer as a function of a true ( $r$ ) and projected ( $R$ ) distance from the object centre respectively and  $\sigma_r$  is the radial velocity dispersion related to the mass distribution in the object (see Lokas & Mamon 2001, 2003).

The best-fitting  $M_v$  and  $c$  values we obtain from the velocity dispersion profiles for the 3 samples we have considered are given in Table 1. The range of mass values illustrates well how much the estimated parameters depend on the sample of galaxies chosen. We find that for the whole sample, as well as for the intermediate sample the resulting masses are significantly larger than expected. Only the most restrictive sample gives a more reasonable value of  $2.6_{-1}^{+2} \times 10^{15} M_\odot$  (at 68 per cent confidence level), much more in agreement with the value deduced from recent studies based on lensing (Broadhurst et al. 2005a,b). Although this sample may still contain unbound galaxies which bias the result towards higher masses, it is clear that any further division of this sample into two parts of comparable size, as was done by Girardi et al (1997), would result in a mass estimate at least a factor of few lower, strongly at variance with the value estimated from lensing.

Although our best-fitting concentration for this sample is much higher than expected, as in the case of studies based on lensing, the data do not allow us to really constrain the concentration, i.e. all values in the range  $5 < c < 100$  are consistent with the data at  $1\sigma$  level. We emphasize, however, that our cut-offs in velocity were rather arbitrary and although they followed the gaps in the  $v(R)$  diagram it would be difficult to justify them in a quantitative way. In particular, none of the galaxies in the  $v(R)$  diagram in Fig. 1 would be removed by the application of standard methods for the rejection of outliers. This suggests that in agreement with visual impression from the  $v(R)$  diagram, the galaxies with discrepant velocities are not just interlopers but belong to some neighbouring structures.

Our analysis illustrates the difficulties encountered when the standard Jeans approach is uncritically applied to clusters before considering all the possible indications on their dynamical status and/or their environment. As it happens for A1689, it could be that discrepant mass estimates are obtained depending on the sample selection criteria. We note that our sample is a compilation of a few surveys with substantial fraction of spiral galaxies (41 per cent among those with known morphological type). While the sample of Teague et al. (1990) comes from a standard magnitude-limited survey, the selection criteria of those of Balogh et al. (2002) and Duc et al. (2002) were aimed at star-forming galaxies which may bias the sample towards outer regions with more substructure. The analysis of the

**Table 2.** Best-fitting virial masses and concentrations of the simulated halo estimated from the 3D information and from velocity dispersion profiles for different particle samples.

sample	$M_v [10^{14} M_\odot]$	$r_v$ [Mpc]	$c$
3D information	5.4	2.1	9.2
$ v  < 3000 \text{ km s}^{-1}$	22	3.4	5.7
$ v  < 1500 \text{ km s}^{-1}$	4.8	2.0	2.1

cluster dynamics could be significantly improved if a survey of many galaxy redshifts complete up to a given limiting magnitude was available. This would allow for a proper comparison with other well studied clusters and a more accurate description of its velocity distribution.

### 3 COMPARISON WITH $N$ -BODY SIMULATIONS

In this section we make use of the  $N$ -body simulations to study the origin of complex velocity distributions like the one in A1689. For this work we used the results of a cosmological dark matter simulation described by Wojtak et al. (2005). The simulation was performed within a box of size  $150 h^{-1}$  Mpc assuming the concordance cosmological model ( $\Lambda$ CDM) with parameters  $\Omega_M = 0.3$ ,  $\Omega_\Lambda = 0.7$ ,  $h = 0.7$  and  $\sigma_8 = 0.9$ . The final output of the simulation contained a few tens of massive haloes found with standard FOF procedures. To mimic observations we place an imaginary observer at a given distance from the halo and project the particle velocities along the line of sight and their positions on the surface of the sky. Among the most massive haloes we chose one with a similar line-of-sight velocity distribution as is seen in A1689. The virial mass of the halo is  $5.4 \times 10^{14} M_\odot$  and it has about  $10^4$  particles inside the virial radius which allows us to reliably measure the density profile. The properties of the halo are summarized in Table 2.

Out of all particles seen by our observer in the direction of the halo inside the projected radius  $R = r_v$  and with velocities  $|v| < 3000 \text{ km s}^{-1}$  with respect to the mean velocity of the halo we randomly select 200 particles to have a similar statistics as for A1689. (The velocity range corresponds to about  $4\sigma_{\text{los}}$  for a halo of this mass.) The summary of the observed properties of the halo is presented in Fig. 2 with the panels analogous to those in Fig. 1 for A1689. The  $v(R)$  diagram in the upper left panel is highly irregular with particle velocities spread out over the whole velocity range and making it difficult to decide which of them should be treated as true members of the halo. A distinct structure is seen at about  $v = 2500 \text{ km s}^{-1}$  which is even better visible in the upper right panel showing the line-of-sight velocity histogram. As for A1689 we separate the particles using the velocity criterion; those with  $|v| < 1500 \text{ km s}^{-1}$  are marked with black dots in the plots while those with  $|v| > 1500 \text{ km s}^{-1}$  with green or blue dots depending on the sign of the velocity. The lower left panel shows the positions of the particles belonging to different velocity bins on the surface of the sky.

The lower right panel of Fig. 1 plots the velocity dispersion profiles calculated from the data from all particles (blue) and only from those with  $|v| < 1500 \text{ km s}^{-1}$  (black). As for A1689 we did a similar exercise of fitting these data with the solutions of the Jeans equation (1) as-

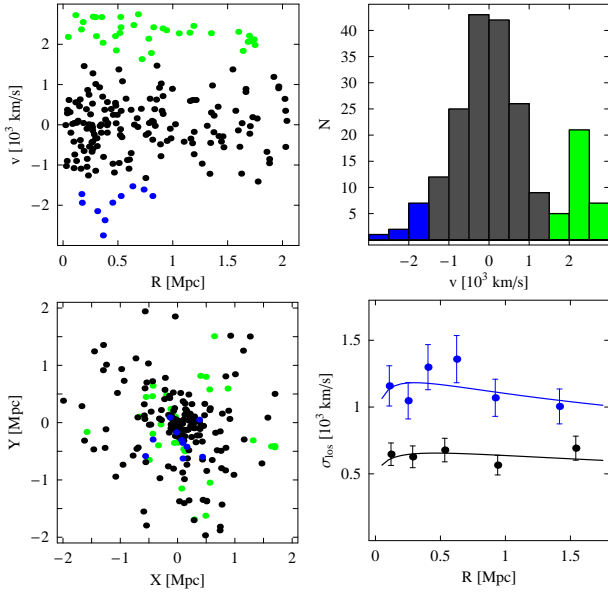


**Figure 2.** Projected distributions of galaxies in the vicinity of the simulated cluster. Upper left panel: line-of-sight velocities of 200 halo particles as a function of projected distance from the halo centre divided into different velocity bins  $|v| > 1500 \text{ km s}^{-1}$  (green and blue respectively for the positive and negative velocities) and  $|v| < 1500 \text{ km s}^{-1}$  (black). Lower left panel: positions of the groups of particles on the surface of the sky. Upper right panel: the histogram of the line-of-sight velocity distribution plotting the number of particles per velocity bin of size  $500 \text{ km s}^{-1}$  with colours coded as in previous plots. Lower right panel: line-of-sight velocity dispersion profiles obtained for all galaxies (blue) and galaxies with  $|v| < 1500 \text{ km s}^{-1}$  (black). Solid lines show the best-fitting solutions of the Jeans equation.

suming isotropic orbits and adjusting the virial mass and concentration. The results for different samples are listed in Table 2. As we can see, the estimated parameters differ dramatically depending on the sample. For the sample with  $|v| < 1500 \text{ km s}^{-1}$  the virial mass is  $M_v = 4.8_{-1.6}^{+1.4} \times 10^{14} M_\odot$  (at 68 per cent confidence level) which agrees well with the mass  $M_v = 5.4 \times 10^{14} M_\odot$  known from the 3D information about the halo. The concentration proves more difficult to estimate with such a small sample and simple modelling since we get  $c = 2.1_{-1}^{+5}$  (at 68 per cent c.l.) which does not include the true value  $c = 9.2$ .

What is the reason behind the complicated velocity structure of the halo? The actual spatial distribution of the particles in a part of the observed region is shown in projection in Fig. 3. The centre of our halo is located at  $x = 0, z = 0$ . The line of sight of the observer is along the  $z$  axis of the plots. The second, smaller halo of mass  $M_v = 8 \times 10^{13} M_\odot$  contributing to the  $v(R)$  diagram shown in Fig. 2 is located at the distance of 45 Mpc from the main halo. As before, we marked the particles with line-of-sight velocities  $v < 1500 \text{ km s}^{-1}$  (with respect to the mean velocity of the main halo) with black dots and those with larger velocities with green ones. Left panel shows all particles in this region of the simulation box, while the right one about 200 chosen randomly to create the mock data (not all 200 particles are shown because the region in the direction of negative  $z$  is not plotted).

The Figure demonstrates that in spite of their proxim-

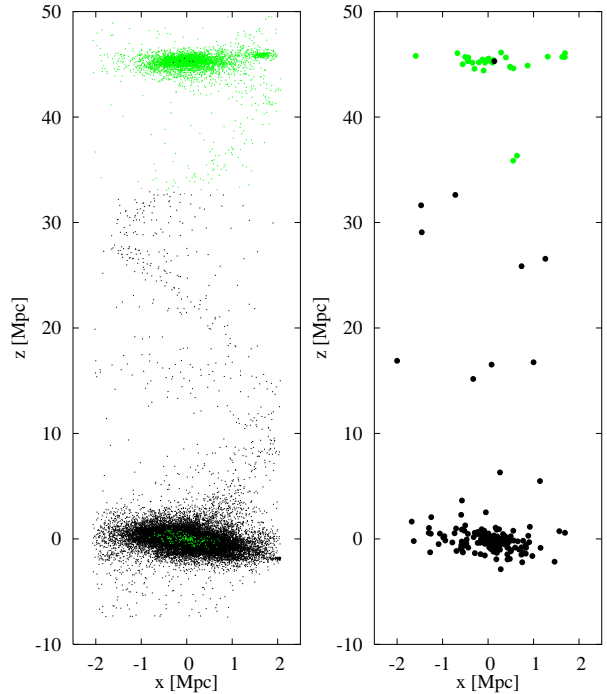


**Figure 3.** Projection of the distribution of dark matter particles in the vicinity of the simulated halo. The main halo is located at  $x = 0, z = 0$ . The observation is done along the  $z$  axis. The second, smaller halo is located at the distance of 45 Mpc from the main halo. The particles with line-of-sight velocities  $v < 1500 \text{ km s}^{-1}$  with respect to the mean velocity of the main halo are coded with black dots, those with larger velocities with green ones. Left panel shows all particles, while the right one about 200 chosen randomly to create the mock data. The flattening of the haloes is due to different distance scales along the two axes.

ity in velocity space ( $2300 \text{ km s}^{-1}$  is of the order of  $3\sigma_{\text{los}}$  of the big halo) the two haloes are in fact very distant. The distance of the smaller halo, 45 Mpc, corresponds to about 20 virial radii of the big halo therefore the haloes do not affect each other dynamically and are not bound to each other, but still their projected velocity distributions are entangled (note that there are green particles in the centre of the bigger halo and black particles in the centre of the smaller halo). The reason for this is the rather low value of the Hubble velocity in comparison with velocity dispersion of bound structures, e.g. velocity dispersions of massive haloes or galaxy clusters are comparable to the Hubble flow at distances as large as 8 virial radii from their centres (see Fig. 3 of Wojtak et al. 2005). The smaller halo in our example is receding from the bigger one with a velocity of about  $2300 \text{ km s}^{-1}$  mainly due to the Hubble flow which at distance of 45 Mpc is of the order of  $3000 \text{ km s}^{-1}$ .

To further illustrate the point, we provide an example of a well-behaved  $v(R)$  diagram. Fig. 4 shows again the  $v(R)$  diagram of our simulated halo from Fig. 2 in the left panel, while in the right panel we present an analogous plot of line-of-sight velocities as a function of projected distance for 200 particles chosen from the same halo, but observed in a different direction. In this case the halo has no massive neighbours along the line of sight and the single particles with discrepant velocities can be easily dealt with using standard procedures for interloper removal.

Our purposely chosen example illustrates well the diffi-

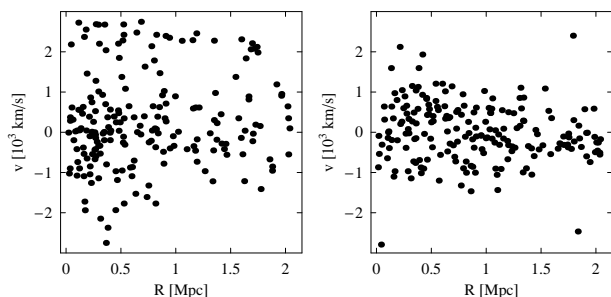


**Figure 4.** Comparison of line-of-sight velocities of dark matter particles as a function of projected distance from halo centre. Left panel shows the same diagram as in upper left panel of Fig. 2. Right panel shows the  $v(R)$  diagram for the same halo observed in a different direction. Both panels plot 200 randomly selected particles.

culties in interpreting the measured line-of-sight velocities of galaxy clusters in the case of presence of neighbouring structures. Whereas velocity differences amounting up to  $2300 \text{ km s}^{-1}$ , as in our simulated haloes, could easily be interpreted as orbital velocities of dynamically bound objects, they could also correspond to structures seen in projection but otherwise separated by distances much larger than their virial radii and, therefore, totally unrelated.

To make a connection with the studies based on lensing we note that the surface density distribution (the main lensing observable) measured along the line of sight in our simulations is increased by about 25 percent everywhere along the projected radius of the bigger halo due to the presence of the smaller halo. The significance of this effect will of course depend on the exact properties of the haloes and probability of their alignment, which will be studied elsewhere.

#### 4 CONCLUSIONS

We have shown that cosmological structures quite distant from each other, when aligned with the direction of observation, can produce projected velocity distributions which are quite difficult to interpret. In particular, such extended distributions can lead to very different velocity dispersion, and therefore mass, estimates. The complicated structure of the velocity distribution, with many peaks, suggests however that we indeed deal with multiple objects situated along the line of sight. On the other hand the simulations show that close neighbours, within one virial radius from each other (like mergers or infalling subhalo), have similar velocities and would produce regular, one-peak velocity distributions.

Given the multi-peak velocity structure of A1689 we conclude that the groups of galaxies with  $\pm 4000 \text{ km s}^{-1}$  (and of course also the more discrepant group at  $+8000 \text{ km s}^{-1}$ ) with respect to the cluster mean velocity are probably separate structures not associated with the cluster, but aligned along the line of sight. If the velocities  $\pm 4000 \text{ km s}^{-1}$  are due mainly to the Hubble flow these structures are located at about 60 Mpc from the cluster. For a cluster mass of  $2 \times 10^{15} M_{\odot}$  the distance corresponds to about 17 virial radii. This would mean that the structures do not affect the cluster dynamically and cannot be responsible for any departures from equilibrium. This rather complex structure in velocity does not necessarily translate itself into the X-ray gas distribution that can appear regular and smooth. This is indeed the case for A1689, in which the morphology of the

X-ray data is commonly interpreted as a clear indication of the relaxed state of the cluster. Andersson & Madejski (2004) demonstrate however that in the case of two similar clusters aligned along the line of sight X-ray data can easily underestimate the mass by a factor of 2.

The presence of foreground and background structures in the line of sight of A1689 may affect the path of light coming from the lensed galaxies. In their study of strong lensing in A1689 Broadhurst et al. (2005a) managed to subtract the neighbouring structure from the main lensing signal. However, no such correction was made when the analysis was extended by Broadhurst et al. (2005b) to weak lensing and larger distances from the cluster centre. Hoekstra (2003) has shown that even the presence of distant large-scale structure in the Universe can affect the weak lensing signal, significantly increasing the uncertainty in the estimated parameters for a given cluster. A similar increase in the estimated errors was shown to be the case if the cluster departs from spherical symmetry (Oguri et al. 2005). It would be interesting to verify whether objects in the vicinity of the cluster could cause similar effect, thereby decreasing the claimed discrepancy with CDM structures, especially when the weak lensing signal is very low and the inferred surface mass distribution in the outer regions very uncertain, as in the case of A1689 (Broadhurst et al. 2005b).

#### ACKNOWLEDGEMENTS

We wish to thank T. Broadhurst, H. Hoekstra and the anonymous referee for their comments on the paper. Computer simulations presented in this paper were performed at the Leibnizrechenzentrum (LRZ) in Munich. EL is grateful for the hospitality of Instituto de Astrofísica de Andalucía in Granada where part of this work was done. RW acknowledges the summer student program at Copernicus Center. This research has made use of the NASA/IPAC Extragalactic Database (NED) operated by the Jet Propulsion Laboratory. This work was partially supported by the Polish Ministry of Scientific Research and Information Technology under grant 1P03D02726 and the exchange program of CSIC/PAN.

#### REFERENCES

- Andersson K. E., Madejski G. M., 2004, *ApJ*, 607, 190
- Balogh M. L., Couch W. J., Smail I., Bower R. G., Glazebrook K., 2002, *MNRAS*, 335, 10
- Broadhurst T. et al., 2005a, *ApJ*, 621, 53
- Broadhurst T., Takada M., Umetsu K., Kong X., Arimoto N., Chiba M., Futamase T., 2005b, 619, L143
- Bullock J. S., Kolatt T. S., Sigad Y., Somerville R. S., Kravtsov A. V., Klypin A. A., Primack J. R., Dekel A., 2001, *MNRAS*, 321, 559
- Duc P. A. et al., 2002, *A&A*, 382, 60
- Girardi M., Fadda D., Escalera E., Giuricin G., Mardirossian F., Mezzetti M., 1997, *ApJ*, 490, 56
- Hoekstra H., 2003, *MNRAS*, 339, 1155
- Lokas E. L., Mamon G. A., 2001, *MNRAS*, 321, 155
- Lokas E. L., Mamon G. A., 2003, *MNRAS*, 343, 401
- Navarro J. F., Frenk C. S., White S. D. M., 1997, *ApJ*, 490, 493
- Oguri M., Takada M., Umetsu K., Broadhurst T., 2005, *ApJ*, 632, 841
- Struble M. F., Rood H. J., 1999, *ApJS*, 125, 35
- Teague P. F., Carter D., Gray P. M., 1990, *ApJS*, 72, 715
- Wojtak R., Lokas E. L., Gottlöber S., Mamon G. A., 2005, *MNRAS*, 361, L1